THE JOURNAL OF PHYSICAL CHEMISTRY B

Article

pubs.acs.org/JPCB

Mechanistic Insights into Phosphopeptide–BRCT Domain Association: Preorganization, Flexibility, and Phosphate Recognition

Yu-ming M. Huang, Myungshim Kang, and Chia-en A. Chang*

Department of Chemistry, University of California, Riverside, California 92521, United States

Supporting Information

ABSTRACT: Promiscuous proteins are commonly observed in biological systems, for example, in modular domains that recognize phosphopeptides during signal transduction. This promiscuous recognition is of fundamental interest in chemistry and biology but is challenging when designing phosphopeptides *in silico* for cell biology studies. To investigate promiscuous recognition and binding processes of phosphopeptides and the modular domain, we selected a domain essential in breast cancer—the breast-cancer–associated protein 1 (BRCA1) C-terminal (BRCT) repeats as our model system. We performed molecular dynamics simulations and detailed analyses of the dihedral space to study protein fluctuation and conformational changes with phosphopeptide binding. We also studied the association processes of phosphorylated and unphosphorylated peptides using Brownian dynamics with a coarse-grained model. We found that the BRCT domain is preorganized for phosphopeptide binding but has a moderate arrangement of side chains to form complexes with various types of phosphopeptides. Phosphopeptide binding restricts the system motion in general, while the nonpolar phosphopeptide becomes more flexible in the bound state. Our analysis found that the BRCT domain utilizes different mechanisms, usually termed lock and key, induced-fit, and population-shift/conformational-selection models, to recognize peptides with different features. Brownian dynamics simulations revealed that the charged phosphate group may not always accelerate peptide association processes, but it helps the phosphopeptide orient into binding pockets accurately and stabilizes the complex. This work provides insights into molecular recognition in the promiscuous protein system.

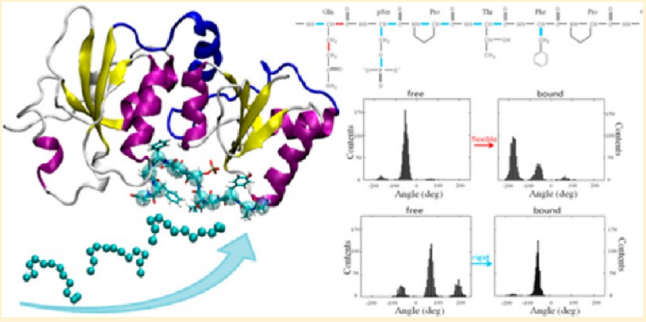

INTRODUCTION

Promiscuous proteins are biological receptors that can successfully interact with a number of different partners at the same binding interface.[1−5] Several modular domains, such as FHA, WW, SH3, and PDZ, can interact with more than one peptide sequence.[6−11] Understanding these protein−peptide interactions is of great interest in a wide variety of applications such as molecular detection, inhibitor discovery, and searching for binding partners. Promiscuous recognition at the molecular level usually involves large conformational changes and numerous bond rotations.[12,13] However, the underlying mechanism that drives diverse ligands to dock into the same binding site of a protein is not fully understood. One vital modular domain system—the breast-cancer–associated protein 1 (BRCA1) C-terminal (BRCT) repeat—shows strong binding affinity with different types of phosphoserine (pSer) peptides.[14]

The BRCA1-BRCT repeats are associated with essential tumor suppressor functions, including DNA repair, cell-cycle checkpoint, and transcription regulation.[15−18] Previous studies have shown that missense mutations in the BRCT domain increase the susceptibility to ovarian and breast cancer.[19,20] A single domain in the BRCT fold is packed with four parallel β sheets with a pair of α helices (α1 and α3) flanked on each side and one helix on the opposite face (Figure 1a).[21] The overall structure of the dual-repeats BRCT domain of different proteins is conserved; a cluster of hydrophobic residues locates at the interface between the two repeats.[14] Both structure and simulation studies indicated that the mutations along the dimer and binding interface could abolish the BRCT functions. Unlike the BRCT domain, the linker connecting the two repeats is more diverse, with poorly defined crystal structures, which suggests flexibility of the linker region.[22]

Several BRCT−peptide complex cocrystal structures are available, and the bound peptides BRCH1, CtIP, and ACC1 were obtained by library screening (Table 1).[23−27] All the cocrystal structures are similar and show the phosphopeptide bound in a groove that involves both N- and C-terminal repeats (Figure 1a). The binding pocket recruits peptides with the conserved motif pSer-X-X-Phe, where X denotes any residue.[28,29] The pSer-binding site is composed of the residues, including a Ser-Gly motif in the β1−α1 connecting loop and a Thr-X-Lys motif at the N-terminus of α2 in the same repeat. The phenylalanine is recognized by a highly hydrophobic cavity located at the interface between the N- and C-terminal

Received: May 23, 2012
Revised: July 31, 2012
Published: August 3, 2012

dx.doi.org/10.1021/jp305028d | J. Phys. Chem. B 2012, 116, 10247−10258

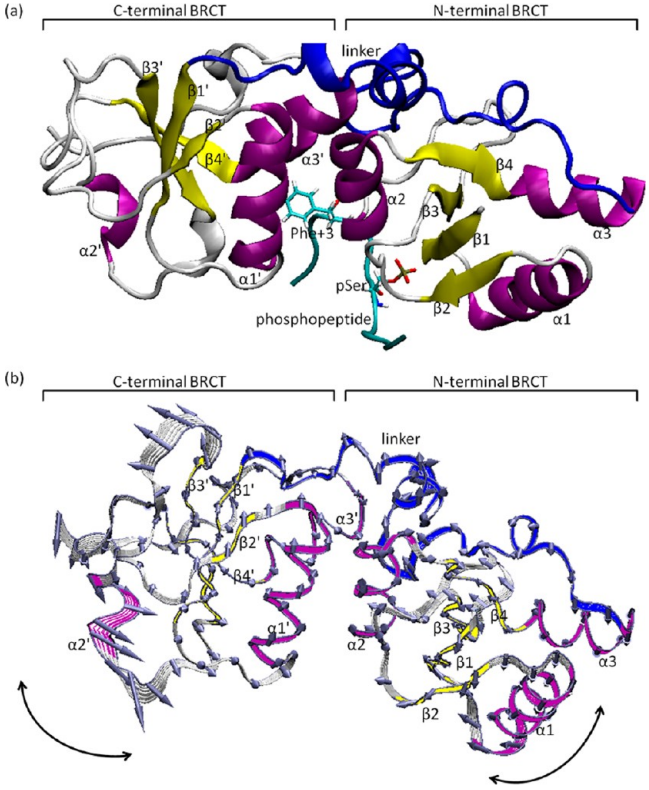

Figure 1. (a) One molecular dynamics (MD) snapshot of the structure of the BRCA1-BRCT domain. The α-helix, β-sheet, and linker are in purple, yellow, and blue, respectively. (b) Principle component analysis (PCA) of 50 ns MD simulation. The gray arrows indicate the local direction and magnitude of movement, and the black arrows represent overall movement direction.

Table 1. Peptide Sequences from Domain−Phosphopeptide Complexes[a]

no.	PDB ID	protein	K_d (μM)	sequence	reference
1	1T2V	screening	0.4	AAYDI**pS**QVFPFA	26
2	1T29	BACH1	0.9	ISRST**pS**PTFNKQ	24
3	1Y98	CtIP	3.7	PTRVS**pS**PVFGA	27
4	3COJ	ACC1	5.2	PQ**pS**PTFPEAG	25
5	1JNX	BRCA1		free domain	21

[a]The major binding residues, pSer and Phe+3, are in bold. Other residues with non-polar contributions are underlined.

domains; thus, both repeats are necessary for the BRCA1-BRCT−peptide binding.[26,30] However, except for the model sequence pSer-X-X-Phe, sequences of phosphopeptide are diverse. Both polar and nonpolar residues can generate effective affinity for recognition.[31,32] In addition to analyzing crystal structures, solution NMR has been used to characterize the movement between BRCA1-BRCT and the corresponding phosphopeptide of BACH1, despite no structure output in NMR dynamic studies.[33,34]

Conformational changes play an important role in molecular recognition. The analysis of protein−ligand interactions has been typically divided into three representative postulates: lock and key, induced-fit, and population-shift/conformational-selection model.[35,36] The basic mechanism of the lock and key model has been introduced for a while.[37] In this postulate, only correctly preorganized substrates are capable of fitting into the active site of the lock, which indicates that the conformations would not change during binding (Figure 2a).[38−40] Since not all cases can be adequately explained by the rigid lock model, another assumption, induced-fit theory, has been proposed and showed that biomolecules are rather flexible structures in which the conformation can be reshaped and distorted to form optimal interactions with partners (Figure 2b).[36,38,41] In recent years, experiments support another mechanism, termed population shift or conformational selection model. In this model, a large number of conformations has pre-existed in the native state; after binding fluctuations perturb the structure, and the properties of population switch (Figure 2c).[36,42] Here, we examined these models by analyzing conformational transitions in several BRCT domain−peptide systems using molecular dynamics (MD) simulations.

The MD method has been widely used to study binding mechanisms in different domain−peptide systems such as PDZ, SH2, SH3, and FHA.[43−48] The energy calculations with MD trajectories provide insight into the driving force of phosphopeptide binding.[44,46,49−51] Moreover, mutation studies with MD simulations have explained how mutating a single residue can diminish phosphopeptide binding.[46,47] For example, Gough et al. studied several BRCT mutants by MD simulation.[20] Here, we address questions of promiscuous recognition in the binding of various phosphopeptides and tandem BRCT repeats. We performed MD simulations and carried out detailed analysis of the dihedral space to study protein fluctuations with free and bound BRCT repeats, conformational changes of the domain and peptide with phosphopeptide binding, and interaction energy between promiscuous phosphopeptides and BRCT. Because the charged phosphate group might play an important role in the early stage of molecular recognition, we also used Brownian dynamics (BD) simulations with coarse-grained (CG) models to study the encounter processes with phosphopeptides and non-phosphopeptides.

MATERIALS AND METHODS

Molecular Systems. In this work, we selected one apo and four holo forms of the tandem BRCA1-BRCT repeats to study binding promiscuity. The initial coordinates for all systems were taken from known crystal structures in the Protein Data Bank (PDB) database. We explored the structure of the apo domain, PDB 1JNX (resolution 2.50 Å), and one complex with a screening phosphopeptide, PDB 1T2V (resolution 3.30 Å).[21,26] We studied the other three holo structures in complex with phosphopeptides from BRCH1, CtIP, and ACC1 proteins with PDB IDs 1T29 (resolution 2.30 Å), 1Y98 (resolution 2.50 Å), and 3COJ (resolution 3.21 Å), respectively.[24,25,27] The substrate peptide sequences are in Table 1. Moreover, we performed an MD simulation for one more free BRCT domain by manually removing the phosphopeptide from the 1T2V complex, and we expected the simulation results to be similar to those initiated from the free domain, PDB 1JNX. Similarly, we performed multiple MD simulations for four free phosphopeptides by directly taking their 3D coordinates from the cocrystal structures with the BRCT repeats.

MD Simulation Protocol. We performed MD simulations on two apo domains, four complexes, and four free phosphopeptides to study the dynamic nature of a given system. The standard simulation packages, Amber10 and NAMD2.6, with the Amber 99SB force field, were used.[52−55] Because the parameters of the phosphoresidues are not defined

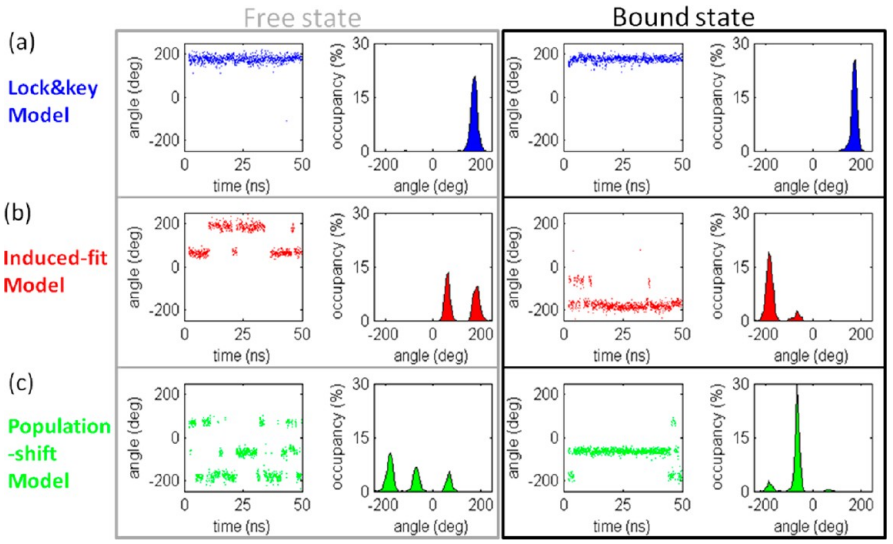

Figure 2. Three models to represent conformational changes before and after peptide binding. We considered the specific dihedral angle during 50 ns MD simulations and plotted it as a histogram distribution. Sampled data are from pSer-2nd-side chain angle in peptide 3 (a), Arg-1st-side chain angle in peptide 3 (b), and Arg-3rd-side chain angle in peptide 2 (c).

in a typical Amber force field, we used the pSer force field reported by Homeyer et al.[56] All systems were sampled separately with the following procedure. First, we checked the protonation state by using the MCCE program.[57,58] After a quick energy minimization for 100 steps, the systems were solvated in a rectangular box of 12 Å explicit TIP3P water model by the tleap program in the Amber10 package.[59] Each system contains about 50 000 atoms. Placement of the counterions of Na^+ was based on the Coulombic potential to keep the whole system neutral, and particle mesh Ewald was used to consider long-range electrostatic interactions.[60] Before equilibration, we ran energy minimization of 10 000 and 20 000 steps for the waters and the system, respectively; then, the systems were gradually heated from 250 K for 20 ps, 275 K for 20 ps, and 300 K for 200 ps. We collected the resulting trajectories every 1 ps with a time step of 2 fs in the isothermic−isobaric (NPT) ensemble. The Langevin thermostat with a damping constant of 2 ps^{-1} was employed to maintain a temperature of 300 K, and the hybrid Nosé−Hoover Langevin piston method was used to control the pressure at 1 atm. We also used the SHAKE procedure to constrain hydrogen atoms during MD simulations.[61] Finally, all production runs were performed for 50 ns (got 5000 snapshots, time period 0.01 ns) at 300 K. To ensure that all simulations reached stable energy fluctuations, we considered only trajectories in the 2−50 ns range for postanalysis. Root-mean-square deviation (rmsd) and root-mean-square fluctuation (RMSF) were measured by use of the VMD program and Bio3D package, respectively.[62,63]

Interaction Energy Calculations. To quantify thermodynamic information of domain−peptide interactions, we used the molecular mechanics/Poisson−Boltzmann surface area (MM/PBSA)-type post processing method to compute ligand−protein intermolecular energy without strain entropy based on the MD structure ensemble.[12,64−70] Since it does not consider entropic changes in ligand binding, we also applied the T-Analyst program using the Gibbs formula to compute configurational entropy as described in next section. The total energy (E_{tot}) can be decomposed into two terms: potential energy (U) and solvation energy (W). The potential energy can be further divided into valence (bond, angle, and dihedral) (U_v), van der Waals (U_{vdw}), and Coulombic (U_{Coul}) energy; also, the solvation term includes the polar contribution evaluated by the Poisson−Boltzmann equation (W_{PB}) and the nonpolar term with cavity/surface area energy (W_{np}). The change in interaction energy was calculated as follows:

$$\Delta E_{tot} = \Delta U_v + \Delta U_{vdw} + \Delta U_{Coul} + \Delta W_{PB} + \Delta W_{np} \quad (1)$$

The binding energy computed here includes the solvation free energy, which considers water entropy. Calculation of the W_{PB} and W_{np} terms was based on PBSA and the solvent-accessible surface area (SASA) model, respectively, in the sander program of Amber 11.[69] We used 40 Å as a cutoff for nonbonded interactions in all energy calculations. The dielectric constants of the interior and exterior protein were set to 1 and 80, respectively.

The interaction energy (ΔE_{bind}) associated with the binding of a domain and its conjugated phosphopeptide in forming a complex is represented as follows:

$$\Delta E_{bind} = \langle E_{complex} \rangle - \langle E_{bound.domain} \rangle - \langle E_{bound.peptide} \rangle \quad (2)$$

The bracket $\langle E \rangle$ denotes the average energy computed from a given MD trajectory. Note that the valence energies are canceled out in eq 2 because of the single trajectory approach. Because the intermolecular charged attractions and polar solvation energy usually compensate for each other, we summed the U_{Coul} and W_{PB} terms as net electrostatic interaction (E_{polar}). The total contribution of nonpolar energy (E_{np}) can also be considered as the combination of U_{vdw} and W_{np}. Thus, the binding energy can be represented as follows:

$$\Delta E_{bind} = \Delta E_{polar} + \Delta E_{np} \quad (3)$$

Entropy Calculation. We considered the configurational entropy S from each dihedral angle, which includes both conformational and vibrational parts, reflecting the number of energy wells and the average width of the occupied wells, respectively.[71−73] Calculation of the configurational entropy was based on the bond-angle-torsion (BAT) coordinate, and the total entropy could be decomposed into an individual

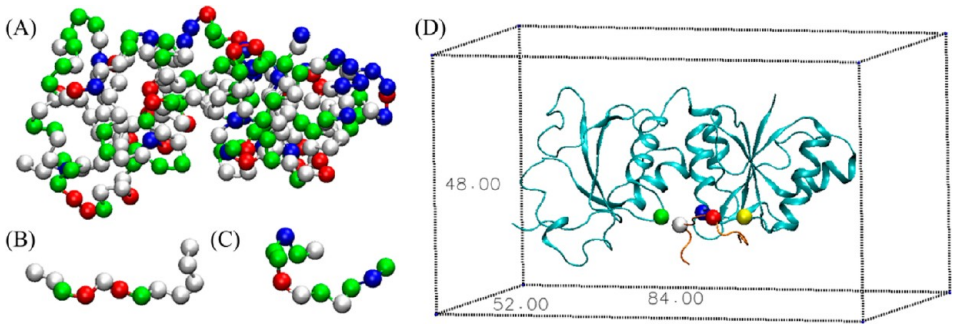

Figure 3. Coarse-grained representations and criteria of steps 1 and 2 in peptide−domain association: (A) BRCT domain; (B) peptide 1; (C) peptide 2. The acidic, basic, polar, and nonpolar residues are in red, blue, green, and white, respectively. The sizes shown do not reflect the actual sizes. (D) For step 1, the encounter box is a rectangular box 84 × 48 × 52 Å^3 around the BRCT domain. The BRCT domain and peptide are in cyan and orange, respectively. The five residues used to determine the distances for step 2 are represented by spheres: pSer and Phe+3 in the peptide are red and white, respectively, and Gly1656, Arg1699, and Asn1774 in the domain are yellow, blue, and green, respectively.

dihedral term, including backbone (phi, psi, and omega) and side chain. The following Gibbs entropy formula was used to calculate torsional entropy:

$$S = -R \int p(x) \ln p(x)\, dx \tag{4}$$

where $p(x)$ is the probability distribution of each dihedral angle x and R is the gas constant. We demonstrated all entropy calculations by use of T-Analyst.[74] Only the internal dihedral degree of freedom for each rotatable bond was considered, and the coupling between dihedrals was ignored. The change in configuration entropy between peptide-bound and -free states can be presented as follows:

$$T\Delta S_X = TS_{X,\text{bound.state}} - TS_{X,\text{free.state}} \tag{5}$$

where X denotes each dihedral angle, such as phi, psi, omega, and side chain.

To ensure $p(x)$ converges during 50 ns MD, we compared the trajectories between 2 and 47 ns, 2 and 48 ns, and 2 and 50 ns to make sure that the computed dihedral entropy is converged.

Principal Component Analysis. Principal component analysis (PCA) involves computing a linear transformation to map data from a high dimension to a lower order space.[75,76] PCA allows for statistical representation of a set of random variables. Two steps are usually involved in the calculation: stepping up a covariance matrix of projected positions and diagonalizing this matrix. The covariance matrix of a given data set can be written as follows:

$$C_{ij} = \langle (x_i - \langle x_i \rangle)(x_j - \langle x_j \rangle) \rangle \tag{6}$$

where x_i and x_j denote each atom position and bracket $\langle x \rangle$ is the mean value of the MD ensemble. The diagonalization of the sample covariance matrix can be efficiently estimated on an orthogonal basis by finding its eigenvalues (λ) and corresponding eigenvectors ($\mathbf{A}$) as follows:

$$\mathbf{A}^T\mathbf{C}\mathbf{A} = \lambda \tag{7}$$

The first PCA mode, PCA1, is the projected subset of the first deviation position. This number has high variance and represents the greatest possible number of motions. We used the Bio3D package for all PCA calculations, including first, second, and third modes, based on the coordinate of Cα carbon atoms.[63] The final results were visualized and plotted by use of the VMD program.[62]

Identify Different Conformations. To identify conformational changes of a molecule, we analyzed the rotamer states of each dihedral angle from the MD trajectories. The analysis with T-Analyst involved 5000 frames from each 50 ns MD simulation.[74] The degree of each dihedral (x), including phi, psi, omega, and side chain, was computed, and the population of each dihedral was generated by use of Matlab with a histogram of 72 bins. We then manually defined the range of each energy well (rotamer state) of a dihedral based on the computed population (details are in the Text S1 section of the Supporting Information). Different conformations can be clearly described with the defined energy wells. For example, one molecule has two dihedrals, A and B. The dihedral A has two dihedral populations, A1 and A2. The dihedral B has three populations, B1, B2, and B3. Conformation #1 was considered dihedral A and B of one MD snapshot staying in the A1−B1 energy well. Other snapshots with similar structure staying in the A1−B1 energy well were clustered with conformation #1. Otherwise, they were new conformations. Because the omega angles stay in the single energy well and the other two backbone angles, phi and psi, are usually in one or two energy wells, we focused on changes in side chains.

Coarse-Grained Model. For studying the early stage phosphopeptide−domain association, we used CG models to represent the BRCT domain and peptides 1 and 2 (Figure 3). In our CG model, a single interaction center was placed on the Cα to represent each residue and connected by virtual bonds, angles, and dihedral angles.[77−79] Formal integer charges were assigned to the charged residues, including pSer. The detailed procedure was described previously.[80] The domain was held rigid, and the peptide was fully flexible. Nonbonded intramolecular interactions within the peptide consisted of a pseudo-Morse bond to model the van der Waals interactions with a 15 Å cutoff. Coulombic interaction was $U_{\text{elec}} = q_iq_j/\varepsilon_{ij}r_{ij}$, where r_{ij} is the distance between beads i and j. To avoid unrealistic Coulombic interactions, a distance-dependent dielectric constant ($\varepsilon_{ij} = 4r_{ij}$) was used. Nonbonded intermolecular interactions were represented by the Lenard-Jones type potential, $U_{\text{vdw}} = 0.5[((r_i + r_j)/r_{ij})^8 - 1.5((r_i + r_j)/r_{ij})^6]$, where r_i and r_j are the effective radii of beads i and j, respectively.[81] The effective radii were taken from van der Waals radii calculated previously.[82] Manual assignment of the effective radii of residues in the peptide and binding site of BRCT was based on the crystal structures (Table S1, Supporting Information). The radius of pSer of the peptides

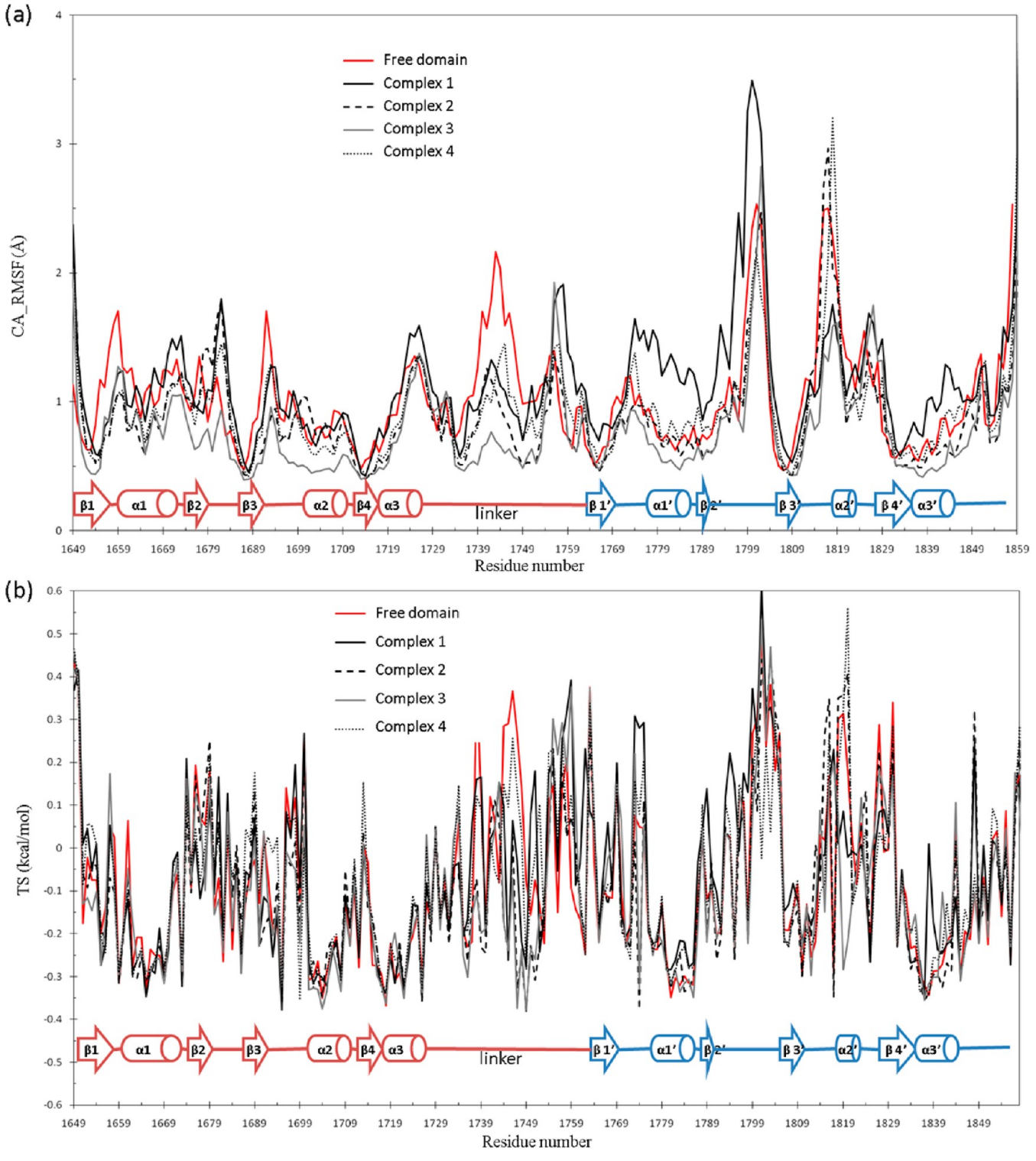

Figure 4. (a) Root mean square fluctuation (RMSF) of Cα atoms. (b) Entropic distributions of backbone phi torsion angles from the free domain and four complexes in 50 ns MD simulations.

was set to be the same as that of Ser, but pSer had a −2 formal charge assigned in the Cα. Reference structures for BRCT were taken from a snapshot at 5 ns for peptide 1 and at 2 ns for peptide 2 in the atomistic simulation.

Brownian Dynamics Approach. The Brownian dynamics (BD) simulations with CG models can provide appropriate time scales to study diffusive association of the domain and peptides.[83,84] The modified UHBD software package was used in the simulations.[85,86] The time step was 50 fs, with a maximum simulation time of 40 μs. The trajectory was saved every 1 ns.

The system is a sphere with a radius of 160 Å. The BRCT domain was located at the center of the sphere. Each simulation was initiated with a single peptide on the surface of the bounding sphere, with a different initial position or different random number of seeds. BD simulation was then performed

dx.doi.org/10.1021/jp305028d | J. Phys. Chem. B 2012, 116, 10247−10258

until the association criterion for the second step was satisfied (see below). To keep the concentration of the peptide constant, a periodic boundary condition-like conversion was used; i.e., if the peptide escaped the bounding sphere, it was placed diagonally opposite, with an additional pull of 2% total distance toward the center of the sphere to ensure that the peptide stayed inside the sphere. To analyze the effect of phosphorylation step by step, the whole diffusive association process was divided into three steps. The first step involved the peptide approaching the domain by diffusion to make an encounter complex. As a simple expedient, a rectangular box of $84 \times 48 \times 52$ Å^3 was defined around the domain, and once the peptide entered the box, it was considered as reaching the first step. In the second step, the peptide moved inside the binding pocket. We checked three distances based on the relative position of the peptide in the complex to determine whether the peptide was inside the binding pocket: the distance between pSer and Gly1656, Phe+3 residue and Arg1699, and Phe+3 residue and Asn1774 being within 9, 11, and 10 Å, respectively, for peptide 1 and 9, 10, and 25 Å for peptide 2. In addition, for peptide 1, Phe+3 needed to be closer to Arg1699 than pSer to ensure that the peptide was in the correct direction in the pocket. In the third step, the complex reached the final stable conformation, but it was not included in the BD studies because the CG model cannot capture atomistic details, such as forming hydrogen bonds between the phosphate group and BRCT residues. The final step to reach the final bound states needed to be modeled by using atomistic force fields, which we discuss here. During BD simulations, we considered that the system was successfully associated when the criteria for the first and second steps were fulfilled.

RESULTS AND DISCUSSION

To further understand molecular recognition and help provide strategies for designing binding partners, we investigated how promiscuous peptides bind to the same target groove of tandem BRCT domains. We selected the BRCA1-BRCT domain in complex with four different phosphopeptides. Peptides 1 and 2 contained a large number of hydrophobic and charged residues, respectively, and peptides 3 and 4 contained a combination of polar and nonpolar residues (Table 1). Notably, despite sequence variety, all peptides showed similar binding affinity, with K_d values ranging from 0.4 to 5.2 μM.

Overall Dynamics of the Free BRCT Domain. Protein dynamics can provide information for understanding protein function and ligand recognition; however, directly probing the dynamic behavior experimentally is challenging. Thus, MD simulation is an effective tool to assess protein motion. Before proceeding with more detailed analysis, we checked the root-mean-square deviation (rmsd) (Figure S1, Supporting Information) to confirm that all simulations achieved equilibrium. The rmsd showed that backbone atoms moved within approximately 0.5 to 1.0 Å. Then, we focused on several key contacts between the BRCT repeats and their conjugated phosphopeptides. In general, the interactions between the domain and individual peptides from our MD simulations agreed with the experimental results. The MD trajectories for the four complexes showed each peptide positioned in a groove that extended across both BRCT repeats. pSer located in a shallow pocket of the N-terminal BRCT domain, whereas Phe +3 located in a hydrophobic cavity at the interface between two dimer subsets. Tight interactions between the BRCT domain and peptide primarily involved residues from pSer to Phe+3. The residues of the extended peptide N- and C-terminus were less close to the BRCT domain for complexes 1 and 4. However, in addition to mainly two-knob binding, several residues such as Thr1658, Glu1660, Lys1690, and Val1740 at the N terminus of complexes 2 and 3 have direct contacts in recognition through both polar (H-bonds) and non-polar (short distance between methyl groups) interactions. The interactions corresponding to each peptide are simplified in Figure S2 of the Supporting Information, which indicates that the binding modes are rather diverse in independent complexes.

As mentioned previously, the BRCT repeats display a unique packing of a tandem structure, with two subunits linked by a flexible loop. Thus, any correlated motion between the subunits could associate with phosphopeptide recruitment, which governs the BRCT functions. We therefore used PCA to analyze MD trajectories and determine whether the movements were related in the inter-BRCT repeats. The first PCA showed the two subunits of the dimer moving in and out (closed and open) together and demonstrated a "grabbing"-like movement through moderate correlations (see arrows in Figure 1b). Notably, the marginal helices, $\alpha1$ and $\alpha2'$, and the loops near the binding site, $\beta1-\alpha1$, $\beta2-\beta3$, and $\alpha1'-\beta1'$, showed in-and-out movement, but the interfolding region, $\beta1$, $\beta2$, $\beta3$, and $\beta4$, showed less movement. These internal dynamics could help sandwich phosphopeptides in a surface cleft between two individual subunits opposite the linker.

Changes in Protein Dynamics with Peptide Binding. To probe the structural changes with peptide binding, we analyzed the RMSF of Cα carbon and configurational entropy of dihedral degrees of freedom to illustrate differences with and without the phosphopeptide. Figure 4 shows that, except for the inter-BRCT linker region and the external loop $\beta2'-\beta3'$ and $\beta3'-\alpha2'$, the backbone of BRCT is in general rigid. The bound and free states did not differ in structure. We further compared the RMSF and entropy plot. The large RMSF of $\beta1'$, $\alpha1'$, $\beta2'$, and $\alpha3'$ of BRCT suggests that these regions of complex 1 are more flexible in the bound state; however, the entropy plot of the phi angles did not show the same results. The same discrepancy was found in $\beta2$, $\alpha2$, $\alpha1'$, $\beta4'$, and $\alpha3'$ of complex 3. Detailed analysis showed that the backbone of these regions was not more mobile than that of other regions. However, the structural shift of small loop regions nearby resulted in larger changes of RMSF for these α-helices or β-sheets in Cartesian space, which may not accurately reflect changes in internal motion. Therefore, the computed torsion entropy can more efficiently capture the changes in a protein's internal movement induced by peptide binding.

To investigate how the same domain can successfully recruit different partners, we focused on the residues of BRCT that directly contact the peptides. Table S2 in the Supporting Information gives changes in single-residue entropy between the peptide-bound and -free states for residues around the binding site. The range of total entropy change of dihedrals ($T\Delta S$) with peptide binding was −5.5 to +3.2 kcal/mol. The entropic changes were mainly from change in side chains, and the backbone was relatively immobile, with small entropy changes, −2.0 to +0.4 kcal/mol, after peptide binding. The minor changes in backbone entropy infer that the BRCT repeats are inflexible in the recognition interface in the free state. This preorganized protein structure can help peptide binding because of the small entropic cost during the formation of the complex.

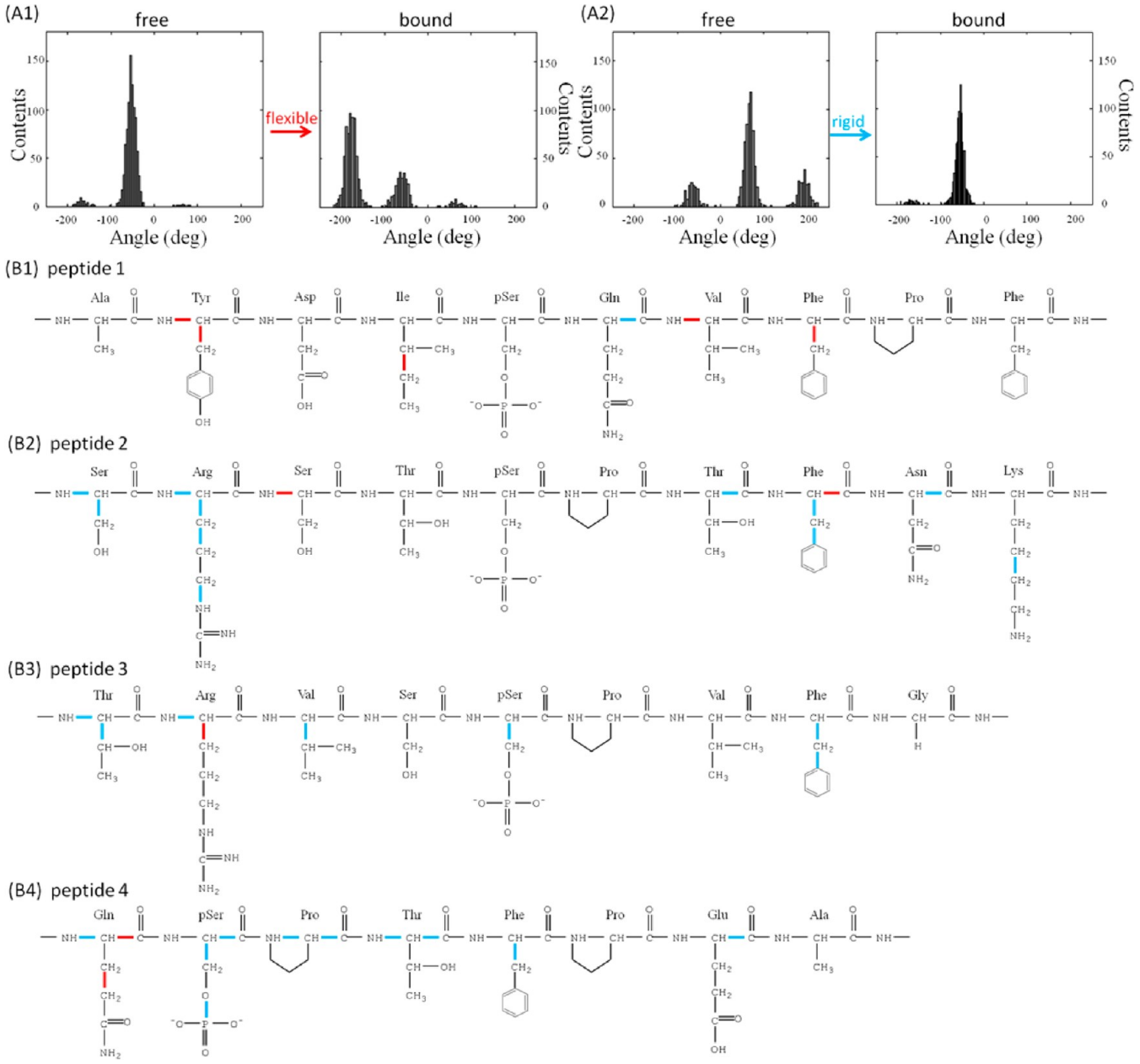

Figure 5. Parts A1 and A2 represent the dihedral angle distribution during 50 ns MD simulation. The four peptide sequences with all rotatable bonds are plotted in parts B1−B4. Red and blue indicate that the conformations become more flexible and rigid, respectively, in the bound state.

Although, in some cases, binding restricts the molecule's movement and reduces configurational entropy, we noticed that the protein from complex 1 was more flexible in the bound than in the free state (entropic gain 3.26 kcal/mol in Table S2, Supporting Information); forming the complex with the nonpolar peptide 1 provided a hydrophobic environment that allowed for adopting different binding conformations. The increase in binding conformations gained entropy and hence drove complex 1 toward the bound state. The favorable entropy is in part from increasing the flexibility of nonpolar residues in the binding site (e.g., Thr1700, Leu1839, Leu1701, and Met1775) (Table S2, Supporting Information). The similar observations of entropy changes were also discussed in existing publications.[12,87−89] However, complexes 2, 3, and 4 showed reduced BRCT flexibility (entropic loss of protein is 3.98, 5.58, and 1.56 kcal/mol, respectively). Although the bound complexes had smaller space for protein fluctuation and therefore were more rigid than the free complexes, new side chain conformations were still able to emerge in the bound state (discussed in the next paragraph), so the capacity for accepting new conformations plays an important role in promiscuous protein binding.

Changes in Dihedral Rotation with Phosphopeptide Binding. Changes in protein dynamics can result from significant changes in protein conformations or from altering the local vibration of many dihedral rotations. Here, we examined the rotamer states of residues in the binding site of BRCT and four phosphopeptides. As expected, for the BRCT domain, the rotamer states of the backbone dihedral angle mostly stayed in a single energy well and remained the same with or without peptide binding. However, the side chain dihedrals were more flexible and usually had more than one

dx.doi.org/10.1021/jp305028d | J. Phys. Chem. B 2012, 116, 10247−10258

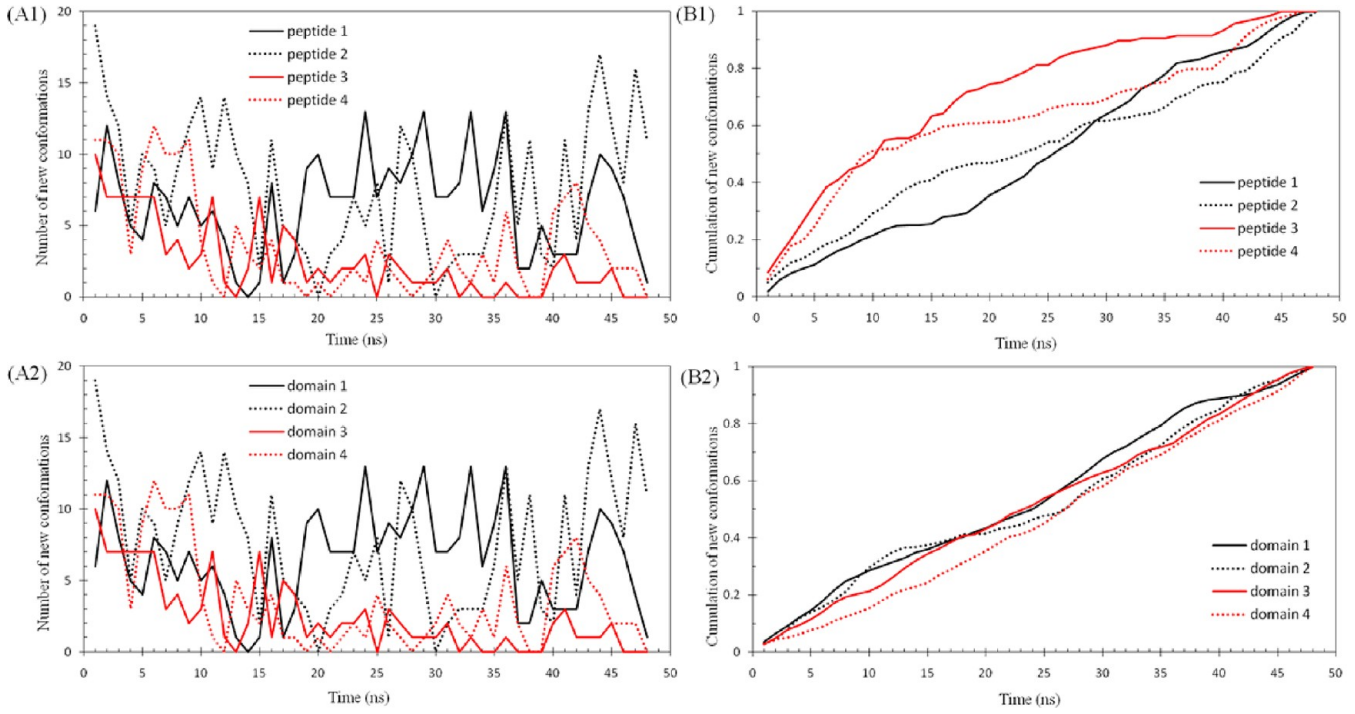

Figure 6. The number of new conformations in the bound state sampled every 1 ns by MD simulation. (A1) The side chain conformations of peptides 1, 2, 3, and 4. (A2) The side chain conformations of the domain from complexes 1, 2, 3, and 4. (B1 and B2) The percentages of new conformations accumulated during simulation of peptides and domain, respectively. For the domain, we considered only the residues around the binding site.

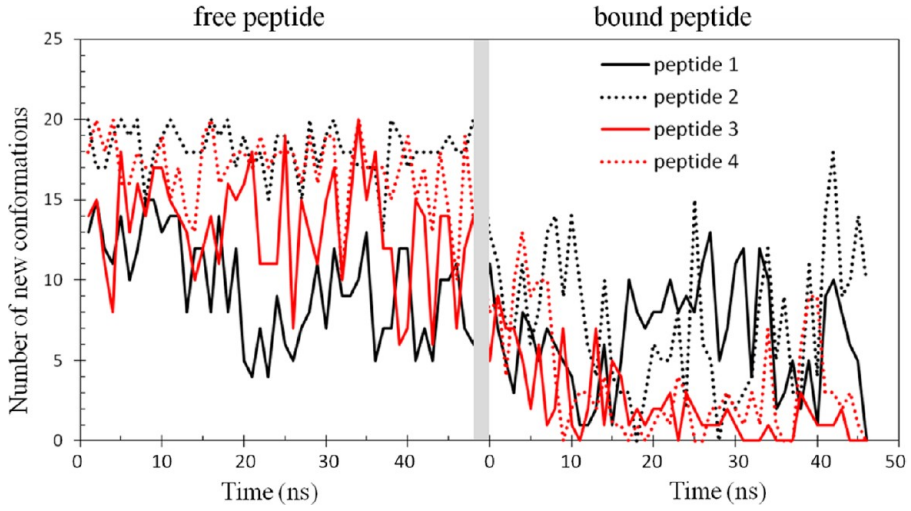

Figure 7. The number of new conformations obtained from the free (left) and bound (right) peptide during 50 ns MD simulation. The conformations were counted every 1 ns.

rotamer state. Table S3 in the Supporting Information shows the dihedral distribution of side chains in the apo domain and bound complexes. Although, commonly, ligand binding decreases the number of available rotamer states (Figure 5A2), the rotamer states of BRCT and the peptides can be increased or decreased or remain unchanged after peptide binding in the bound state (Figure 5A1, B1 and Table S4, Supporting Information). Upon binding to BRCT, residues Tyr-3, Ile-1, Val+2, and Phe+3 of peptide 1 showed new rotamer states, which suggests that the peptide can efficiently rearrange itself to fit into the binding interface of BRCT. New rotamer states of several nonpolar residues of peptide 1 were induced by binding a hydrophobic binding groove, which resulted in increased configuration entropy (~1.7 kcal/mol shown in Table S5, Supporting Information), as mentioned previously. This new dihedral angle distribution is a case that fits in the induced-fit model (Figure 2b). For peptides 2, 3, and 4, despite new rotamer states and different conformations being found in the bound complexes, most dihedral angles were less mobile and had fewer rotamer states, which utilizes the "conformational selection" or "population-shift" mechanism (Figures 2c and 5B2, B3, and B4). Therefore, highly charged (peptide 2) and mixed (peptides 3 and 4) side chains are more flexible in a water environment, but the movement is restrained when the peptides bind to the hydrophobic groove of BRCT. Despite the decreased flexibility of BRCT and the peptides,

dx.doi.org/10.1021/jp305028d | J. Phys. Chem. B 2012, 116, 10247−10258

Table 2. Domain−Phosphopeptide Interaction Energy (kcal/mol) by MM/PBSA Calculation[a]

no.	ΔU_{VDW}	ΔU_{Coul}	ΔW_{PB}	ΔW_{np}	ΔE_{polar}	ΔE_{np}	ΔE_{tot}	$\Delta\Delta E_{tot}$	ΔG_{exp}	$\Delta\Delta G_{exp}$
1	−49.91	−71.42	116.81	36.18	45.39	−13.74	31.66	0.00	−8.84	0.00
2	−62.34	−333.37	384.80	40.24	51.43	−22.09	29.32	−2.34	−8.35	0.49
3	−47.86	−177.95	224.74	33.31	46.79	−14.55	32.24	0.58	−7.50	1.34
4	−55.42	−4.26	56.11	36.01	51.85	−19.41	32.45	0.79	−7.30	1.54

[a] ΔU_{VDW} and ΔU_{Coul} are the van der Waals and electrostatic interactions, respectively; ΔW_{PB} and ΔW_{np} are the polar and non-polar contributions from the solvation energy. ΔE_{polar} represents the sum of ΔU_{Coul} and ΔW_{PB}, and ΔE_{np} represents the sum of ΔU_{VDW} and ΔW_{np}. The total interaction energy, ΔE_{tot}, is the sum of ΔE_{polar} and ΔE_{np}. $\Delta\Delta E_{tot}$ and $\Delta\Delta G_{exp}$ are the energy compared with that from complex 1.

both parties can adopt different conformations for peptide binding through moderate side chain arrangement. Moreover, the population of some side chains of peptides and BRCT does not change during binding and the side chains preorganize as a lock and a key illustrated in Figure 2a.

The combination of different rotamer states produces different protein conformations. Because the backbone is in general rigid and preorganized, we focused on side chain movement during MD simulations. Figure 6 shows that many new conformations were generated every 1 ns in the bound state with MD simulations. We expected that the MD runs would sample more new conformations at the beginning of the simulations, and finding new conformations thereafter would take longer. Surprisingly, for short peptides with only 12−21 rotatable bonds, a similar number of new conformations occurred during 50 ns MD simulations, which suggests that significantly longer MD runs are necessary to thoroughly sample conformations. Because pSer and Phe+3 are key residues for recognition and show H-bond and geometric complementation when forming a complex, we investigated whether the two residues were locked into the conformation shown in the crystal structures. pSer and Phe+3 have a total of five rotatable side chain dihedrals, and new conformations from the two residues still appeared at the end of a 50 ns MD simulation (Figure S3, Supporting Information). The multiple rotameric states from the key residues during the simulations suggest that both the termini and compact core regions retain remarkable mobility in the complexes.

To further study how frequently and how many new conformations are generated with the free and bound peptides, we removed the same conformations in both the free and bound peptides (Figure 7 and Table S6, Supporting Information). Because a conformation is defined by the combination of all rotatable dihedrals (see the Materials and Methods section for details) and a change of rotamer state in any dihedral results in a new conformation, almost all conformations sampled with the bound peptides were considered new (Figure 7). For example, for peptide 1 bound to the domain, we sampled 310 different conformations, and 309 were new. Because new conformations generated in the bound state can differ greatly from those in the free form, predicting the bound peptide conformations can be challenging, especially for peptides with mainly nonpolar residues. More aggressive conformational search tools are needed in addition to classical MD simulation to predict new conformations.

Binding Energy Studied by MM/PBSA. The analysis of interaction energy offers insight into the mechanism of binding, so we analyzed each energy component by MM/PBSA-type calculation to study the driving forces behind the formation of complexes. Table 2 shows the decomposition of interaction energy into electrostatic and nonpolar contributions with intermolecular and solvent attraction; the changes in configuration entropy with binding are not included in the table. Because the configurational entropy changes are not considered in these MM/PBSA-type calculations, the computed energy results ($\Delta\Delta E_{tot}$) may not be comparable with experimental data ($\Delta\Delta G_{exp}$). However, the MM-PBSA-type analysis still provides useful information of decomposed energy. Notably, although all complexes, particularly 2 and 3, show strong Coulombic attraction, the intermolecular attraction is largely compensated by the solvation free energy (W_{PB}).

Of note, the absolute values of the nonpolar solvation term (W_{np}) are highly positive, which results in the unfavorable interaction energy (E_{tot}). This standard error has been previously detected in several protein−ligand systems.[44] However, the relative interaction energy can still reconstruct the correct experimental ranking of binding energy. In addition, a comparison of polar (E_{polar}) and nonpolar (E_{np}) contributions revealed that the entire binding adaption is driven by the preference of hydrophobic interactions. In contrast to the electrostatic effects, the domination of van der Waals contributions reveals that the BRCT repeats mostly interact with nonpolar peptides by their typical hydrophobic groove. This finding is not surprising: this thermodynamic basis of favorable nonpolar and unfavorable electrostatic contributions was observed in similar MM/PBSA studies of PDZ and SH3 domains.[43,44]

Coarse-Grained Brownian Dynamics Simulation of the Phosphorylation Effect on Diffusional Association. Introducing charge interactions between BRCT and the phosphopeptide stabilizes the bound complex. We wondered whether the charged phosphate group accelerates the diffusional association of the peptide. We therefore carried out BD simulations using a CG model to study the effect of phosphorylation on the binding kinetics for two peptides from the phosphate group with and without the negative charge (Table 3 and Figure 3 for the CG models and setup). Our simulations modeled the first two steps of the binding process. The first step is defined as free diffusion from a surface of a sphere, 160 Å away from the domain until the peptide diffuses near BRCT, and this step may be influenced by long-range

Table 3. The Mean Times (μs) for Each Step in the Association of the Peptide and the BRCA1-BRCT Domain[a]

peptide	phosphorylation	net charge[b]	first step	second step	steps 1 and 2	success rate
1	pSer	−3	8.3	14.6	22.6	75%
	Ser	−1	7.3	6.2	13.5	100%
2	pSer	0	5.8	11.8	17.6	83%
	Ser	2	5.8	4.5	10.3	98%

[a] The maximum simulation time was 40 μs, and 200 Brownian dynamics runs were used for each system. [b] Net charge from the peptide. In addition, BRCT has a net charge of −5.

electrostatic attractions. The second step models the details of how the peptide enters the binding site, including lateral diffusion along the domain surface. The second step can be affected by electrostatic interactions, but geometric complementation captured by short-range van der Waals interactions may have an important role in this step.

The BRCT domain carries a −5 unit of formal charge. Adding the phosphate group increased the net charge of the peptide by −2. By increasing the negative charge of peptide 1 from −1 to −3 by adding the phosphate group, BRCT and the phosphorylated peptide 1 needed ∼14% more time to meet each other. In contrast, phosphorylated peptide 2 without the formal charge showed no difference in first encounter time with and without the phosphate group (Table 3). However, it diffused faster than peptide 1. Despite no significant acceleration in the first diffusion step when the peptide has a +2 net charge, carrying negative charges enhanced the electrostatic repulsion and slowed the diffusion process. Unexpectedly, although the phosphate group is essential to form the BRCT−phosphopeptide complex, adding the phosphate group slowed the second step of association. Both peptides took 2−3 times longer to find the binding pocket and orient themselves to the final bound state with phosphate group. The positive-charged residues in the linker region temporarily kept the phosphopeptides locally (Figure 8), and

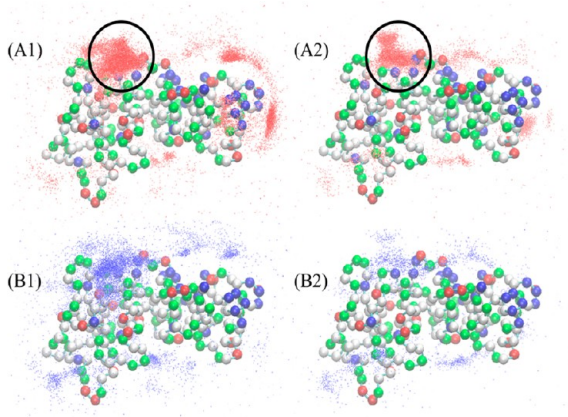

Figure 8. The distribution of charged residues in the BRCT domain and density of peptides 1 and 2. The red dots represent the trajectories of the phosphopeptides 1 (A1) and 2 (A2), and the blue dots represent trajectories of their respective nonphosphorylated counterparts 1 (B1) and 2 (B2). The peptides were saved every 10 ns before entering the binding site. Each system involved 200 runs. The black circles represent the highly positive-charged region where phosphopeptides tend to wander longer than in any other areas. The acidic, basic, polar, and nonpolar residues are in red, blue, green, and white, respectively.

sometimes the peptides stayed there longer than 15 μs (Figure S6, Supporting Information). As a result, the total traffic time along the BRCT surface was increased, thus resulting in a longer BRCT−peptide association process. Moreover, nearly 25 and 17% of phosphopeptides 1 and 2, respectively, could not successfully form a final bound complex within a 40 μs BD simulation.

Of note, proteins containing the BRCT domain may have a considerably different charge distribution on the protein surface. Therefore, the slowdown in the overall BRCT−peptide association by adding the phosphate group could be an artifact of considering only the domain part. However, the results suggest that solely increasing the net charge of a molecular system may not always benefit binding kinetics, and the charge patches on a protein surface may temporarily trap the binding partner. The local effects may be insignificant for protein−protein binding, because their surface contact is typically large and the binding relies highly on protein surface complementation. However, small molecules such as peptides or chemical compounds may spend a considerably long time in a highly charged region, thus slowing down the association process. As a result, systems with fast binding kinetics may need to use electrostatic steering to accelerate ligand diffusion and avoid a small molecule being electrically trapped by regions other than the targeted binding site.

Although the phosphate group is not able to accelerate phosphopeptide association, the charge interactions can efficiently orient the phosphopeptide to form and stabilize the bound BRCT−phosphopeptide complex. During our BD simulations, once the phosphopeptides found the binding site and formed the final bound complex with BRCT, the phosphopeptides stayed in the binding pocket, with small fluctuation, and did not leave BRCT. However, nonphosphorylated peptides fluctuated largely and frequently left BRCT, even after the defined final bound complex was formed (Figure 9 and Figures S5 and S6 in the Supporting Information). Therefore, charge interactions may have an important role in BRCT−phosphoresidue recognition. In biological systems, accurate phosphorylated protein−BRCT recognition plays a crucial role in DNA-damage checkpoints, although the association may not be optimized by kinetics. Notably, BD simulations provide a valuable tool for studying the overall interactions and processes of a biomolecular system. Even though our CG model missed atomistic details, including hydrogen bonds between pSer and residues of BRCT, we could observe the roles of pSer in stabilizing and anchoring the peptide into the binding pocket of the domain.

■ CONCLUSIONS

In this study, we applied molecular dynamics and Brownian dynamics simulations to our model systems, BRCT domain−phosphopeptide complexes, to investigate conformational changes and phosphate recognition during peptide binding. The analysis of dihedral angle examined protein fluctuation and conformational switches. First, from our simulations, the MD results show preorganization of the backbone of BRCT and moderate arrangements of side chain to create an optimal binding environment. Second, three models for explaining molecular recognition were all observed in our simulations. We observed that a part of dihedral angle population does not have significant changes during ligand binding, which is related to the lock and key model. In a more hydrophobic environment in which binding enables nonpolar side chains to have more degrees of freedom to rotate, the recognition of BRCT domain and phosphopeptide tends to proceed by the induced-fit model. However, the population-shift model is commonly found in polar interactions due to charge−charge interactions that have preferred direction. Third, the binding region of both protein and peptide are able to be more rigid and flexible while interacting with polar and nonpolar partners, respectively. Finally, BD simulations with the CG model provide good evidence that the charged phosphate group may not always benefit for binding kinetics, but it helps correctly anchor phosphopeptides to the binding pocket during the binding processes.

dx.doi.org/10.1021/jp305028d | J. Phys. Chem. B 2012, 116, 10247−10258

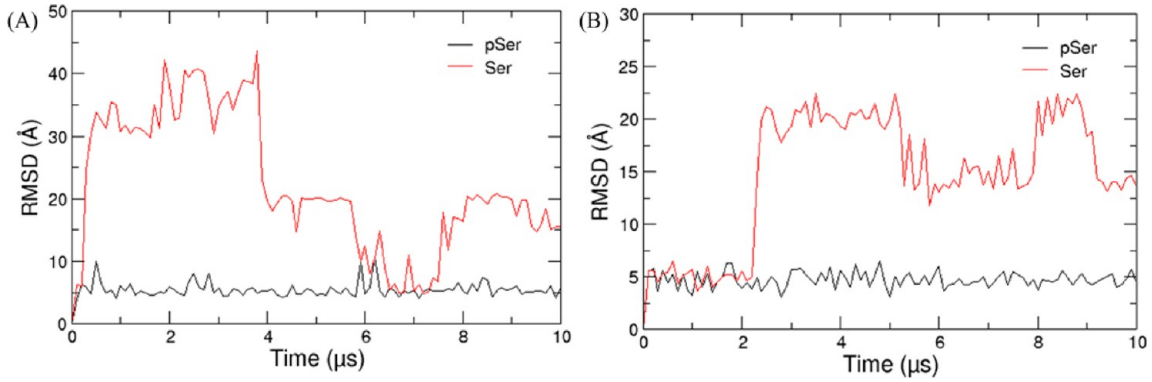

Figure 9. Root-mean-square deviation (rmsd) of Brownian dynamics simulations of the bound peptides 1 (A) and 2 (B) in the binding pocket. The phosphopeptide is in black and nonphosphopeptide in red.

■ ASSOCIATED CONTENT

Supporting Information

Additional figures and tables. This material is available free of charge via the Internet at http://pubs.acs.org.

■ AUTHOR INFORMATION

Corresponding Author

*E-mail: chiaenc@ucr.edu. Phone: (951) 827-7263. Fax: (951) 827-2040.

Notes

The authors declare no competing financial interest.

■ ACKNOWLEDGMENTS

This research was supported in part by start-up funds from the University of California, Riverside, and the National Science Foundation (MCB-0919586) through TeraGrid resources provided by the National Center for Supercomputing (Grant No. TG-MCB080039N) and the University of California Shared Research Computing Services Cluster (ShaRCS), which is supported by multiple UC information technology divisions and managed by the University of California, Office of the President.

■ REFERENCES

(1) Virshup, D. M.; Shenolikar, S. *Mol. Cell* **2009**, *33*, 537.
(2) Nobeli, I.; Favia, A. D.; Thornton, J. M. *Nat. Biotechnol.* **2009**, *27*, 157.
(3) Schreiber, G.; Keating, A. E. *Curr. Opin. Struct. Biol.* **2011**, *21*, 50.
(4) Ma, B. Y.; Shatsky, M.; Wolfson, H. J.; Nussinov, R. *Protein Sci.* **2002**, *11*, 184.
(5) Yuan, P.; Liang, K.; Ma, B.; Zheng, N.; Nussinov, R.; Huang, J. *Chem. Biol. Drug Des.* **2011**, *78*, 137.
(6) Mahajan, A.; Yuan, C. H.; Lee, H.; Chen, E. S. W.; Wu, P. Y.; Tsai, M. D. *Sci. Signaling* **2009**, *2*, re12.
(7) Ilsley, J. L.; Sudol, M.; Winder, S. J. *Cell. Signalling* **2001**, *13*, 625.
(8) Yip, K. Y.; Utz, L.; Sitwell, S.; Hu, X.; Sidhu, S. S.; Turk, B. E.; Gerstein, M.; Kim, P. M. *BMC Biol.* **2011**, *9*, 53.
(9) Kim, H.; Huang, J.; Chen, J. *Nat. Struct. Mol. Biol.* **2007**, *14*, 710.
(10) Liu, B. A.; Jablonowski, K.; Shah, E. E.; Engelmann, B. W.; Jones, R. B.; Nash, P. D. *Mol. Cell. Proteomics* **2010**, *9*, 2391.
(11) Sudol, M.; Bedford, M. T. *Protein Rev.* **2005**, *3*, 185.
(12) Chang, C. E. A.; McLaughlin, W. A.; Baron, R.; Wang, W.; McCammon, J. A. *Proc. Natl. Acad. Sci. U.S.A.* **2008**, *105*, 7456.
(13) Nachman, J.; Gish, G.; Virag, C.; Pawson, T.; Pomes, R.; Pai, E. *PLoS One* **2010**, *5*, e11215.
(14) Glover, J. N. M.; Williams, R. S.; Lee, M. S. *Trends Biochem. Sci.* **2004**, *29*, 579.
(15) Venkitaraman, A. R. *Cell* **2002**, *108*, 171.
(16) Bork, P.; Hofmann, K.; Bucher, P.; Neuwald, A. F.; Altschul, S. F.; Koonin, E. V. *FASEB* **1997**, *11*, 68.
(17) Cantor, S.; Drapkin, R.; Zhang, F.; Lin, Y. F.; Han, J. L.; Pamidi, S.; Livingston, D. M. *Proc. Natl. Acad. Sci. U.S.A.* **2004**, *101*, 2357.
(18) Sancar, A.; Lindsey-Boltz, L. A.; Unsal-Kacmaz, K.; Linn, S. *Annu. Rev. Biochem.* **2004**, *73*, 39.
(19) Coquelle, N.; Green, R.; Glover, J. N. M. *Biochemistry* **2011**, *50*, 4579.
(20) Gough, C. A.; Gojobori, T.; Imanishi, T. *Proteins: Struct., Funct., Bioinf.* **2007**, *66*, 69.
(21) Williams, R. S.; Green, R.; Glover, J. N. M. *Nat. Struct. Biol.* **2001**, *8*, 838.
(22) Watts, F. Z.; Brissett, N. C. *DNA Repair* **2010**, *9*, 103.
(23) Clapperton, J. A.; Manke, I. A.; Lowery, D. M.; Ho, T.; Haire, L. F.; Yaffe, M. B.; Smerdon, S. J. *Nat. Struct. Mol. Biol.* **2004**, *11*, 512.
(24) Shiozaki, E. N.; Gu, L. C.; Yan, N.; Shi, Y. G. *Mol. Cell* **2004**, *14*, 405.
(25) Shen, Y.; Tong, L. *Biochemistry* **2008**, *47*, 5767.
(26) Williams, R. S.; Lee, M. S.; Hau, D. D.; Glover, J. N. M. *Nat. Struct. Mol. Biol.* **2004**, *11*, 519.
(27) Varma, A. K.; Brown, R. S.; Birrane, G.; Ladias, J. A. A. *Biochemistry* **2005**, *44*, 10941.
(28) Manke, I. A.; Lowery, D. M.; Nguyen, A.; Yaffe, M. B. *Science* **2003**, *302*, 636.
(29) Yu, X. C.; Chini, C. C. S.; He, M.; Mer, G.; Chen, J. J. *Science* **2003**, *302*, 639.
(30) Glover, J. N. M.; Williams, R. S.; Lee, M. S. *Trends Biochem. Sci.* **2004**, *29*, 579.
(31) Lokesh, G. L.; Muralidhara, B. K.; Negi, S. S.; Natarajan, A. *J. Am. Chem. Soc.* **2007**, *129*, 10658.
(32) Rodriguez, M.; Yu, X. C.; Chen, J. J.; Songyang, Z. *J. Biol. Chem.* **2003**, *278*, 52914.
(33) Botuyan, M. V. E.; Nomine, Y.; Yu, X. C.; Juranic, N.; Macura, S.; Chen, J. J.; Mer, G. *Structure* **2004**, *12*, 1137.
(34) Joseph, P. R. B.; Yuan, Z.; Kumar, E. A.; Lokesh, G. L.; Kizhake, S.; Rajarathnam, K.; Natarajan, A. *Biochem. Biophys. Res. Commun.* **2010**, *393*, 207.
(35) Koshland, D. E. *Angew. Chem., Int. Ed. Engl.* **1995**, *33*, 2375.
(36) Okazaki, K.-i.; Takada, S. *Proc. Natl. Acad. Sci. U.S.A.* **2008**, *105*, 11182.
(37) Fischer, E. *Ber. Dtsch. Chem. Ges.* **1894**, *27*, 2984.
(38) Lee, B. M.; Xu, J.; Clarkson, B. K.; Martinez-Yamout, M. A.; Dyson, H. J.; Case, D. A.; Gottesfeld, J. M.; Wright, P. E. *J. Mol. Biol.* **2006**, *357*, 275.
(39) Kushwaha, P. S.; Mishra, P. C. *Int. J. Quantum Chem.* **2000**, *76*, 700.
(40) Jorgensen, W. L. *Science* **1991**, *254*, 954.
(41) Koshland, D. E. *Proc. Natl. Acad. Sci. U.S.A.* **1958**, *44*, 98.
(42) Kar, G.; Keskin, O.; Gursoy, A.; Nussinov, R. *Curr. Opin. Pharmacol.* **2010**, *10*, 715.

(43) Hou, T.; Chen, K.; McLaughlin, W. A.; Lu, B.; Wang, W. *PLoS Comput. Biol.* **2006**, *2*, 46.
(44) Basdevant, N.; Weinstein, H.; Ceruso, M. *J. Am. Chem. Soc.* **2006**, *128*, 12766.
(45) Gan, W.; Roux, B. *Proteins: Struct., Funct., Bioinf.* **2009**, *74*, 996.
(46) Huang, Y.-m. M.; Chang, C.-e. A. *BMC Biophys.* **2011**, *4*, 12.
(47) Pennell, S.; Westcott, S.; Ortiz-Lombardia, M.; Patel, D.; Li, J. J.; Nott, T. J.; Mohammed, D.; Buxton, R. S.; Yaffe, M. B.; Verma, C.; Smerdon, S. J. *Structure* **2010**, *18*, 1587.
(48) Kong, Y.; Karplus, M. *Proteins: Struct., Funct., Bioinf.* **2009**, *74*, 145.
(49) Hou, T.; Wang, J.; Li, Y.; Wang, W. *J. Chem. Inf. Model.* **2011**, *51*, 14.
(50) Amaro, R. E.; Cheng, X.; Ivanov, I.; Xu, D.; McCammon, J. A. *J. Am. Chem. Soc.* **2009**, *131*, 4702.
(51) Rapp, C.; Kalyanaraman, C.; Schiffmiller, A.; Schoenbrun, E. L.; Jacobson, M. P. *J. Chem. Inf. Model.* **2011**, *51*, 2082.
(52) Okur, A.; Strockbine, B.; Hornak, V.; Simmerling, C. *J. Comput. Chem.* **2003**, *24*, 21.
(53) Hornak, V.; Abel, R.; Okur, A.; Strockbine, B.; Roitberg, A.; Simmerling, C. *Proteins: Struct., Funct., Bioinf.* **2006**, *65*, 712.
(54) Phillips, J. C.; Braun, R.; Wang, W.; Gumbart, J.; Tajkhorshid, E.; Villa, E.; Chipot, C.; Skeel, R. D.; Kale, L.; Schulten, K. *J. Comput. Chem.* **2005**, *26*, 1781.
(55) Case, D. A.; Cheatham, T. E.; Darden, T.; Gohlke, H.; Luo, R.; Merz, K. M.; Onufriev, A.; Simmerling, C.; Wang, B.; Woods, R. J. *J. Comput. Chem.* **2005**, *26*, 1668.
(56) Homeyer, N.; Horn, A. H. C.; Lanig, H.; Sticht, H. *J. Mol. Model.* **2006**, *12*, 281.
(57) Song, Y. F.; Gunner, M. R. *J. Mol. Biol.* **2009**, *387*, 840.
(58) Song, Y.; Mao, J.; Gunner, M. R. *J. Comput. Chem.* **2009**, *30*, 2231.
(59) Jorgensen, W. L.; Chandrasekhar, J.; Madura, J. D.; Impey, R. W.; Klein, M. L. *J. Chem. Phys.* **1983**, *79*, 926.
(60) Essmann, U.; Perera, L.; Berkowitz, M. L.; Darden, T.; Lee, H.; Pedersen, L. G. *J. Chem. Phys.* **1995**, *103*, 8577.
(61) Ryckaert, J. P.; Ciccotti, G.; Berendsen, H. J. C. *J. Comput. Phys.* **1977**, *23*, 327.
(62) Humphrey, W.; Dalke, A.; Schulten, K. *J. Mol. Graphics Modell.* **1996**, *14*, 33.
(63) Grant, B. J.; Rodrigues, A. P. C.; ElSawy, K. M.; McCammon, J. A.; Caves, L. S. D. *Bioinformatics* **2006**, *22*, 2695.
(64) Sitkoff, D.; Sharp, K. A.; Honig, B. *J. Phys. Chem.* **1994**, *98*, 1978.
(65) Tsui, V.; Case, D. A. *Biopolymers* **2000**, *56*, 275.
(66) Bashford, D.; Case, D. A. *Annu. Rev. Phys. Chem.* **2000**, *51*, 129.
(67) Meirovitch, H. *Curr. Opin. Struct. Biol.* **2007**, *17*, 181.
(68) Wang, J.; Cai, Q.; Li, Z. L.; Zhao, H. K.; Luo, R. *Chem. Phys. Lett.* **2009**, *468*, 112.
(69) Ye, X.; Wang, J.; Luo, R. *J. Chem. Theory Comput.* **2010**, *6*, 1157.
(70) Swanson, J. M. J.; Henchman, R. H.; McCammon, J. A. *Biophys. J.* **2004**, *86*, 67.
(71) Karplus, M.; Kushick, J. N. *Macromolecules* **1981**, *14*, 325.
(72) Levy, R. M.; Karplus, M.; Kushick, J.; Perahia, D. *Macromolecules* **1984**, *17*, 1370.
(73) Chang, C. E.; Potter, M. J.; Gilson, M. K. *J. Phys. Chem. B* **2003**, *107*, 1048.
(74) Ai, R.; Fatmi, M. Q.; Chang, C.-e. A. *J. Comput.-Aided Mol. Des.* **2010**, *24*, 819.
(75) vanAalten, D. M. F.; Conn, D. A.; deGroot, B. L.; Berendsen, H. J. C.; Findlay, J. B. C.; Amadei, A. *Biophys. J.* **1997**, *73*, 2891.
(76) Pearson, K. *Philos. Mag.* **1901**, *2*, 559.
(77) Tozzini, V. *Curr. Opin. Struct. Biol.* **2005**, *15*, 144.
(78) Trylska, J.; Tozzini, V.; McCammon, J. A. *Biophys. J.* **2005**, *89*, 1455.
(79) Muller-Plathe, F. *ChemPhysChem* **2002**, *3*, 754.
(80) Tozzini, V.; McCammon, J. A. *Chem. Phys. Lett.* **2005**, *413*, 123.
(81) Chang, C.-E. A.; Trylska, J.; Tozzini, V.; McCammon, J. A. *Chem. Biol. Drug Des.* **2007**, *69*, 5.
(82) Kim, Y. C.; Hummer, G. *J. Mol. Biol.* **2008**, *375*, 1416.
(83) Ermak, D. L.; McCammon, J. A. *J. Chem. Phys.* **1978**, *69*, 1352.
(84) Gorfe, A. A.; Chang, C.-E. A.; Ivanov, I.; McCammon, J. A. *Biophys. J.* **2008**, *94*, 1144.
(85) Davis, M. E.; Madura, J. D.; Luty, B. A.; McCammon, J. A. *Comput. Phys. Commun.* **1991**, *62*, 187.
(86) Kang, M.; Roberts, C.; Cheng, Y.; Chang, C.-e. A. *J. Chem. Theory Comput.* **2011**, *7*, 3438.
(87) Ma, B. Y.; Tsai, C. J.; Nussinov, R. *Biophys. J.* **2000**, *79*, 2739.
(88) Diehl, C.; Engstrom, O.; Delaine, T.; Hakansson, M.; Genheden, S.; Modig, K.; Leffler, H.; Ryde, U.; Nilsson, U. J.; Akke, M. *J. Am. Chem. Soc.* **2010**, *132*, 14577.
(89) Barratt, E.; Bronowska, A.; Vondrasek, J.; Cerny, J.; Bingham, R.; Phillips, S.; Homans, S. W. *J. Mol. Biol.* **2006**, *362*, 994.